PERGAMON

International Journal of Heat and Mass Transfer 45 (2002) 37–45

International Journal of HEAT and MASS TRANSFER

www.elsevier.com/locate/ijhmt

A new correlation for turbulent mass transfer from liquid droplets

Madjid Birouk *, Iskender Gökalp

Laboratoire de Combustion et Systèmes Réactifs, Centre National de la Recherche Scientifique, 47071 Orléans Cedex 2, France

Received 8 March 2001; received in revised form 3 April 2001

Abstract

This paper presents a new correlation for mass transfer from single liquid droplets into a turbulent environment. Experiments were carried out under ambient room temperature and pressure. Homogeneous isotropic turbulence with zero-mean velocity was generated by eight identical electrical fans placed on the eight corners of a cubic chamber. The LDV technique was used to characterize the turbulence inside the chamber. The vaporization of fiber suspended droplets of five different *n*-alkanes and the bi-component droplet of *n*-heptane and *n*-decane mixtures subjected to varying turbulent kinetic energy is investigated by imaging techniques. For mono-component droplets the d^2-law holds for all fuels and turbulent kinetic energies, and the vaporization rates increase with increasing the turbulent kinetic energy. Bi-component droplets exhibit a sequential vaporization behavior for all mixtures and turbulent kinetic energies. The instantaneous vaporization rates increase with increasing turbulence kinetic energy and increasing volume fraction of the highest volatility component. The proposed correlation predicts the vaporization rates of mono and bi-component *n*-alkane droplets subjected to isotropic turbulence with zero-mean velocity.

Keywords: Droplet vaporization; Mass transfer; Isotropic turbulence; LDV

1. Introduction

The vaporization rate of fuel droplets is the controlling mechanism in many spray combustion applications [1–4]. The formation and the homogeneity of the reactive mixture in diesel and liquid fueled rocket engines, and pre-vaporized premixed combustors essentially depend on the vaporization characteristics of fuel droplets. Moreover, one important ignition and stabilization mechanism of spray flames is due to the formation of a premixed mixture by the rapid vaporization of small droplets near the atomizer nozzle [5]. Most spray combustion devices operate in the turbulent regime and gas phase turbulence may strongly affect the droplet gasification characteristics. In addition, in high pressure liquid fueled combustion devices, the coherence of droplet surface layers is lost due to the reduction of surface tension [6], so that surface stripping may be strongly enhanced by turbulence. In a different but still combustion related area, fire suppression by water mists, the rapid vaporization of water mist droplets is mostly triggered by turbulence. Therefore, examples of two-phase combustion applications where turbulence effects on droplet vaporization matter are numerous. Yet, the development of the basic knowledge on these effects is in its early stage.

Most of the existing knowledge on droplet vaporization in turbulent convective flows relies on early correlations, where the effect of mean convection was lumped together with that of turbulence [7,8]. The review papers on droplet vaporization and combustion are generally silent on the subject. One exception is [9], where a classification of turbulent droplet gasification regimes is attempted. However, a persistent belief is that no turbulence effect is to be expected if energetic turbulence scales (typically the integral length scale) are

* Corresponding author. Present address: Department of Mechanical and Industrial Engineering, University of Manitoba, Winnipeg, Manitoba, Canada R3T SV6.

E-mail address: biroukm@cc.umanitoba.ca (M. Birouk).

0017-9310/02/$ - see front matter
PII: S0017-9310(01)00120-X

Nomenclature

d	droplet diameter
D_L	liquid-phase mass diffusivity
D_m	molecular diffusivity of fuel vapor in air
D_T	turbulent diffusivity
$K(t)$	instantaneous vaporization rate, $d(-d^2)/dt$
K	average vaporization rate
L	turbulent integral length scale
N	fan speed
$Pe_L(t)$	instantaneous Peclet number, $K(t)/D_L$
q	turbulent kinetic energy
Re_t	turbulent Reynolds number, $q^{1/2}d_0/v_a$
Sc	Schmidt number, v_a/D_m
$\Im$	integral time scale
t	time
U, u'	mean and fluctuating velocities along X-axis
V, v'	mean and fluctuating velocities along Y-axis

Greek symbols

v	kinematic viscosity
η	Kolmogorov length scale
λ	Taylor length scale
τ	dissipation time scale

Subscripts

a	air
0	initial
1,2	first and last vaporization sequences in the case of bi-component fuel
s	stagnant case (without turbulence)
t	turbulent

larger than the droplet diameter. On the other hand, numerical work on droplet vaporization in a turbulent medium essentially focuses on the dispersion of droplets by turbulence and largely ignores the heat and mass transfer processes between the liquid and the gas phases.

The present work aims to provide a comprehensive experimental study and analysis of turbulence effects on the vaporization of mono- and bi-component *n*-alkane droplets, and therefore extends our previous study on the same subject [10,20]. In the present study, turbulence effects are isolated by focusing on a single suspended droplet evaporating at ambient room air temperature and pressure. A controlled/idealized turbulence structure is considered by producing a homogeneous, isotropic and zero-mean velocity turbulent flow field. In the following, we first briefly describe the experimental facility and the diagnostics. The main characteristics of the turbulence field are then briefly summarized. The results and discussion section deals with turbulence effects on the vaporization of pure (mono-component) and bi-component *n*-alkane droplets, where the fuel volatility and composition, together with the turbulent kinetic energy, are systematically varied.

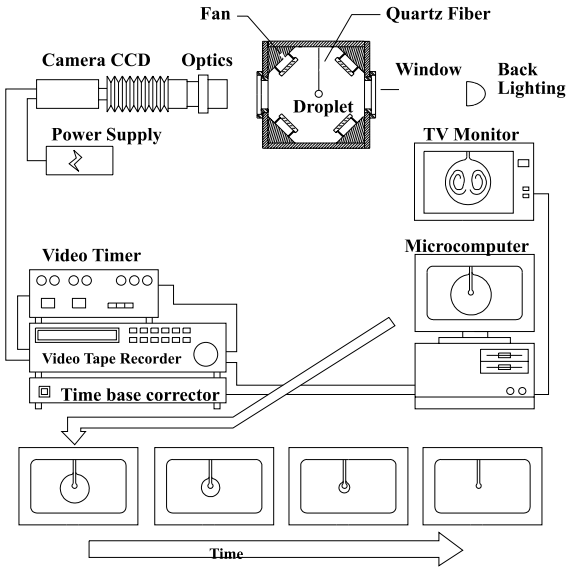

Fig. 1. Schematic representation of droplet visualization and image acquisition system.

2. Experimental facility and diagnostics

Turbulence chambers producing quasi-zero mean velocity turbulence have been used in the past, and are used today, for premixed turbulent propagation studies [11–15]. The turbulence chamber we developed is schematized in Fig. 1. The chamber is cubic with external dimensions of $400 \times 400 \times 400$ mm^3. Internally, the cube corners are designed as shown in Fig. 1, in order to obtain an internal near-spherical volume. Eight electric fans with five blades are fixed in the corners. These fans are capable of generating rotation speed ranging from 750 to 2700 rpm. Four openings and three windows allow access into the chamber, both materially and optically. The chamber is placed on a two-dimensional displacement system [16]. The flow field inside the chamber is characterized using a two-component laser Doppler velocimeter. A 5 W argon-ion laser is the light source, with 0.4 W operating power. The reception optics are arranged in the forward scattering mode with a 14° angle. TSI IFA 750 processors with a Bragg cell are used to determine the instantaneous velocity field. For two-point velocity measurements, a movable second

measuring volume is formed by using a spherical mirror and a second photomultiplier collects the scattered light from the second measuring volume. The flow seeding is obtained by silicon oil drop using an in house made liquid drop generator [16].

A quartz fiber is introduced vertically into the chamber from its topside and is used to suspend a droplet at the center of the chamber (Fig. 1). The quartz fiber is 0.2 mm in diameter and has an enlarged extremity to ease droplet suspension. A single droplet is suspended on the fiber extremity by using a retractable syringe introduced through a hole from one of the lateral windows of the chamber. Droplet initial diameters were of the order of 1.50 mm. The droplets are suspended on the fiber once the turbulence regime is established and then the syringe is retracted. The suspended droplet experiments are inherently subject to the perturbing effects of the suspension fiber [17]. One such effect is the modification of the internal droplet motion patterns. The heat conduction by the fiber is another major effect [18]; in the present room temperature droplet vaporization experiments, this effect is minimized. In general, however, caution is needed when translating the results from suspended droplet experiments to free droplets.

A real time image acquisition and processing system is developed in order to quantify the time variation of the droplet projected surface area and to deduce the droplet vaporization and burning rates under various turbulence conditions. Droplets are backlighted to allow a high contrast between the droplet and the surrounding medium [19]. The time variation of the projected surface area of the droplets is calculated from digitized droplet contours. This information is used to deduce the time variation of the squared equivalent droplet diameter, $d^2(t)$, and the instantaneous droplet vaporization rates as $-\mathrm{d}(d^2)/\mathrm{d}t$, from which averaged vaporization rates are obtained as $\sum_{i=1}^{n}(\Delta d^2/\Delta t)_i/n$, where n is the number of time intervals (Δt) taken for deriving Δd^2.

3. Results and discussion

3.1. Characterization of the turbulence field

The flow structure generated by the fans has been systematically characterized for several fan speeds. Fig. 2 shows the variation of the velocity fluctuations u' and v' and of the square root of turbulent kinetic energy $(q^{1/2} = \sqrt{1.5u'^2})$ with the fan speed, at the center of the chamber (where $u' = v'$ are the r.m.s. values of the corresponding velocity fluctuations; the third component w', not shown here, behaves similarly to the two others). A linear increase of both velocity fluctuations and the turbulence intensity with the fan speed is observed. The same figure also confirms that the global isotropy factor

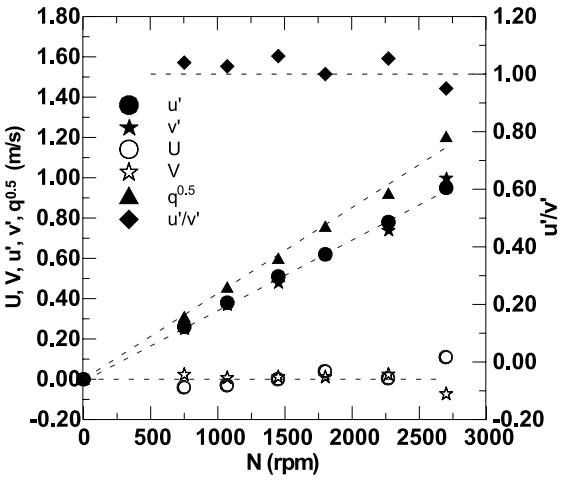

Fig. 2. Variation of the mean and fluctuating flow velocities, square root of the turbulent kinetic energy and u'/v' with fan speed, at the center of the turbulence chamber.

u'/v' is practically equal to 1. It has also been shown that the spectral isotropy is valid for the entire spectral range [16]. Furthermore, Fig. 2 shows that the mean velocity components U and V are quasi-zero, and are independent of the fan speed. Similar results were obtained throughout a spherical region extending on a 20 mm radius from the center of the chamber.

The spatial homogeneity of the turbulence structure has been verified by performing velocity measurements along two orthogonal axes. The measurements indicate that a homogeneous and isotropic turbulence field corresponding to a volume of 40 mm in diameter is obtained [16,20]. As the droplets are suspended in the middle of this volume and have initial diameters of the order of 1.50 mm, the spatial extension of the homogeneous field is largely satisfactory. The measurements also show that the probability distributions of instantaneous velocities for both components are gaussian distributions, with skewness factors close to 0 and flatness close to 3 [16,20]. It is thus confirmed that the facility is able to produce a homogeneous and isotropic turbulence, with quasi-zero mean velocity.

The spectral density functions of the velocity components show that the inertial subrange becomes more extended with increasing fan speed, or turbulent kinetic energy q. Also with increasing q, the high frequency part of the spectrum that corresponds to smaller scales becomes more energetic [16,20]. The integral time scales are determined from the integration of the auto-correlation functions; they decrease from approximately 37 ms for the lowest turbulent kinetic energy ($q = 0.10\ \mathrm{m^2/s^2}$) to about 10 ms for the highest turbulent kinetic energy ($q = 1.45\ \mathrm{m^2/s^2}$). Dissipation time scales are estimated from the dissipation spectra and are found

Table 1
Turbulence characteristics

N (rpm)	q (m^2/s^2)	$q^{1/2}$ (m/s)	$\Im$ (ms)	τ (ms)	L (mm)	λ (mm)	η (mm)	Re_t
750	0.10	0.32	37.30	6.60	8.10	4.90	0.20	31
1070	0.21	0.46	27.30	4.60	8.60	4.20	0.16	45
1450	0.36	0.60	21.50	3.50	8.30	3.60	0.13	59
1800	0.58	0.76	16.60	2.60	8.90	3.30	0.11	75
2270	0.85	0.92	15.60	2.20	8.60	2.90	0.10	90
2700	1.45	1.20	10.50	1.30	8.90	2.60	0.08	118

to vary between approximately 6.60 and 1.30 ms [16]. Two-point measurements of the instantaneous velocity field were used to determine, by integration of the spatial correlation coefficients, the integral length scales of turbulence for each fan speed. The average value of the integral length scale was found to be equal to 8.60 mm, and to be independent of the fan speed [16,20]. This implies that for the droplet gasification regimes explored here, the ratio between the turbulence energetic/integral length scales and the droplet initial diameter is of the order of 5. Under these turbulence conditions, the turbulence Reynolds number based on the initial droplet diameter varies from approximately 31 to 118. The Kolmogorov length scale, estimated using the relationships for isotropic and homogeneous turbulence, decreases with increasing turbulence energy and is found equal to 200 μm for $q = 0.10\ m^2/s^2$ and to 80 μm for $q = 1.45\ m^2/s^2$, giving a Kolmogorov length scale to initial diameter ratio varying between 0.12 and 0.05 [16]. Table 1 summarizes the turbulence characteristics.

3.2. Turbulence effects on the vaporization of mono-component droplets

Some experimental results dealing with the isotropic turbulence effects on the vaporization of mono-component droplets have been published in [20]; this section presents new and complementary results for the same experimental arrangement and the same conditions of isotropic turbulence. The vaporization characteristics of five *n*-alkane droplets, ranging from *n*-hexane to *n*-decane, subjected to the above-characterized turbulence structures have been studied systematically. For each fuel, the turbulent velocity was increased progressively and the time history of the droplet projected surface area recorded as digitized images. Several experiments (typically five) have been performed for each fuel type turbulence pair, and instantaneous and average vaporization rates determined. By moving from light to heavy hydrocarbons, both the volatility and the binary diffusion coefficient of the fuel vapor decrease. For each fuel investigated, the vaporization rates (K_s) under stagnant conditions were also determined and used as reference.

Fig. 3 shows, in normalized coordinates, the time variation of the projected surface area of *n*-decane droplets for various values of turbulent kinetic energy. This figure shows distinctly that the vaporization process of a *n*-decane droplet is drastically enhanced by increasing turbulent kinetic energy. It is also shown that the regression of the droplet projected surface area with time is linear, except at the very end of the vaporization process (not shown in Fig. 3 but apparent in the case of the *n*-heptane droplet in [20], and other fuels in [16]), where the effects of the suspending fiber are important. Hence, the d^2-law (linear variation of d^2 as a function of vaporization time) remains valid under turbulent vaporization conditions. This allows average droplet vaporization rates (K) to be determined for all turbulent kinetic energies. Fig. 4 shows the instantaneous vaporization rate of *n*-decane for all the turbulent kinetic energies explored here. The continuous increase of the vaporization rate with turbulent kinetic energy and the general validity of the d^2-law are also confirmed by this figure. The constant behavior of the instantaneous vaporization rate for each turbulent kinetic energy also indicates that the continuous increase of the ratio

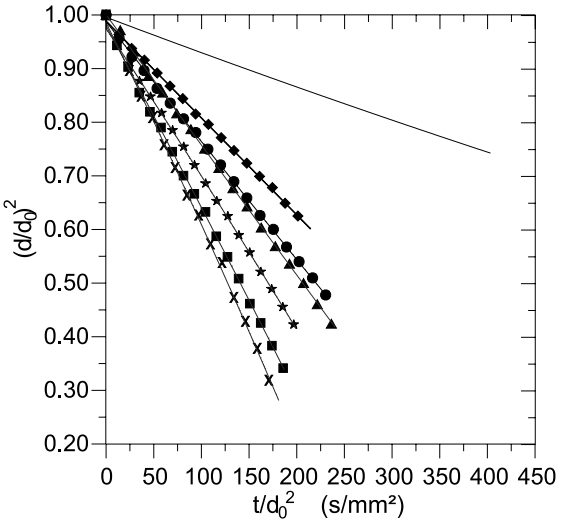

Fig. 3. Time histories of the normalized droplet projected surface area of *n*-decane droplets for various turbulent kinetic energies. (—) Stagnant case; (◆) $q = 0.10\ m^2/s^2$; (●) $q = 0.21\ m^2/s^2$; (▲) $q = 0.36\ m^2/s^2$; (★) $q = 0.58\ m^2/s^2$; (■) $q = 0.85\ m^2/s^2$; (×) $q = 1.45\ m^2/s^2$.

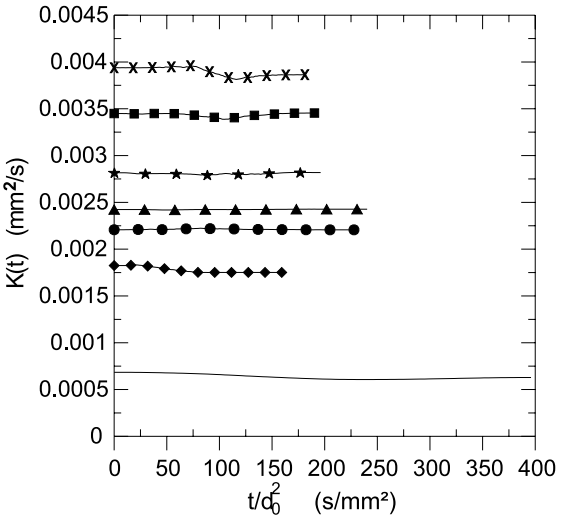

Fig. 4. Instantaneous vaporization rates of *n*-decane droplets for various turbulent kinetic energies (—) Stagnant case; (◆) $q = 0.10$ m^2/s^2; (●) $q = 0.21$ m^2/s^2; (▲) $q = 0.36$ m^2/s^2; (★) $q = 0.58$ m^2/s^2; (■) $q = 0.85$ m^2/s^2; (×) $q = 1.45$ m^2/s^2.

between the turbulence scales and the (decreasing) droplet diameter has no influence on the turbulent droplet vaporization regime explored here. Droplets of *n*-hexane, *n*-heptane, *n*-octane, and *n*-nonane, behave similarly [16,20]. Fig. 5 shows a plot of the normalized average droplet vaporization rates of the five *n*-alkanes explored here versus $Re_t^{2/3}$. Two important observations can be drawn from this figure. First, the averaged normalized rate of each fuel shows a linear variation with $Re_t^{2/3}$. Second, the value of the slope of the linear variation of the normalized averaged vaporization is different for each fuel and increases as the fuel volatility (or molecular diffusivity) decreases. By taking into account the molecular diffusivity of these fuels and hence the Schmidt number, *Sc*, a general expression/correlation was found in which a single linear variation curve of the normalized average vaporization rates of all fuels is plotted as function of $Re_t^{2/3}Sc^2$ (see Fig. 6). The average value of the slope of this correlation is found to be 0.02. The turbulent Reynolds number in this correlation is based on the square root of the turbulent kinetic energy, $q^{1/2}$, and the initial droplet diameter, d_0.

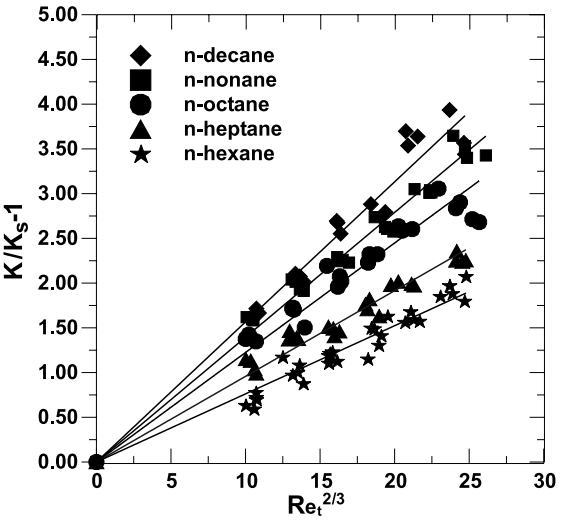

Fig. 5. Variation of the normalized average droplet vaporization rates for five fuels versus $Re_t^{2/3}$.

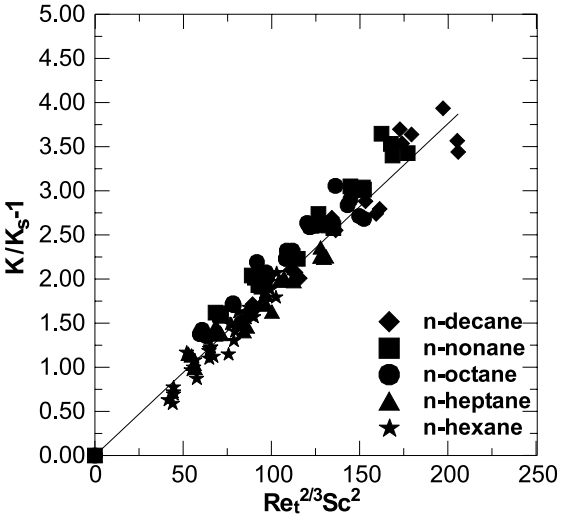

Fig. 6. Variation of the normalized average droplet vaporization rates for five fuels versus $Re_t^{2/3}Sc^2$.

This correlation is purely empirical. The power 2/3 of the Reynolds number is discussed in some early convective heat and mass transfer literature as valid for moderate Reynolds numbers, whereas the classical, or the Frössling type, 1/2 power, is valid for higher Reynolds numbers [21]. The explanation for this power law is elusive. Furthermore, in the present configuration, the Reynolds number is a turbulent one. The generality of the above correlation, proposed to account for the turbulence effects on the vaporization of mono-component droplets, is extended below to the case of bi-component droplets.

3.3. Turbulence effects on the vaporization of bi-component droplets

Turbulent vaporization of bi-component droplets of mixtures of *n*-heptane and *n*-decane has been investigated with the same apparatus and for the same turbulence conditions as for mono-component droplets. The investigated mixtures contain, respectively, 70%, 50% and 30% *n*-heptane by volume. Typical variations of the

normalized squared droplet diameter versus time are shown in Fig. 7 for a mixture with 50% *n*-heptane by volume. The sequential vaporization regime is observed for all turbulence energies, as for the stagnant case, and also, as was observed for the same mixture subjected to a laminar mean convection effect [19]. The corresponding instantaneous vaporization rates are shown in Fig. 8. A short first quasi-steady vaporization sequence is followed by an unsteady vaporization sequence, during which the more volatile *n*-heptane is totally depleted; a quasi-steady vaporization sequence then follows, corresponding to the vaporization of the least volatile component. When compared with mono-component droplet vaporization results, the very initial quasi-steady vaporization rates, K_1, for the bi-component mixture are significantly less than the values for pure *n*-heptane under the same turbulence conditions, indicating that the surface layers are not made up of pure *n*-heptane. The vaporization rates of the second quasi-steady sequence, K_2, are practically identical to those of the less volatile component (*n*-decane) under the same turbulence conditions.

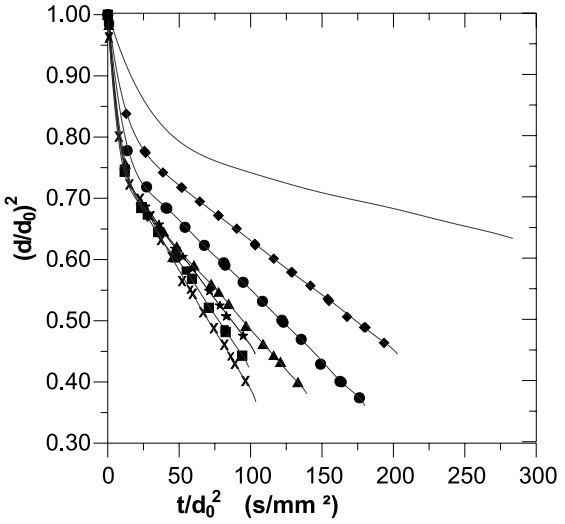

Fig. 7. Time histories of the normalized droplet projected surface area of 50% *n*-heptane/50% *n*-decane mixture droplets for various turbulent kinetic energies (——) Stagnant case; (◆) $q = 0.10\ m^2/s^2$; (●) $q = 0.21\ m^2/s^2$; (▲) $q = 0.36\ m^2/s^2$; (★) $q = 0.58\ m^2/s^2$; (■) $q = 0.85\ m^2/s^2$; (×) $q = 1.45\ m^2/s^2$.

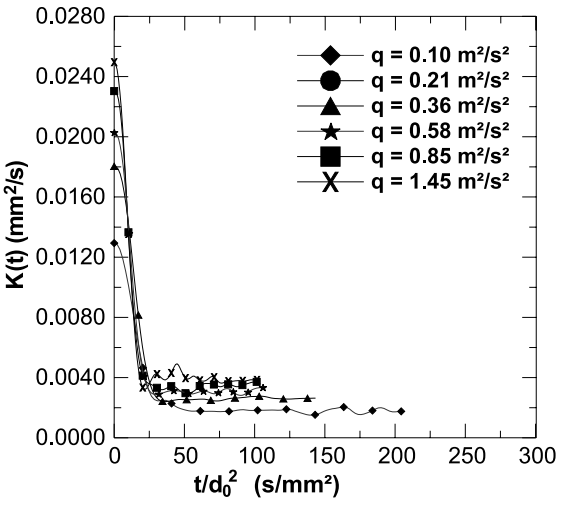

Fig. 8. Instantaneous vaporization rates of 50% *n*-heptane/50% *n*-decane mixture droplets for various turbulent kinetic energies.

Fig. 8 may also be interpreted as an instantaneous Peclet number, $Pe_L(t)$. The instantaneous Peclet number is defined as the ratio of $K(t)$ over D_L, where D_L is the liquid-phase mass diffusivity [22]. For a given mixture, increasing the turbulent kinetic energy increases therefore the Peclet number, and shortens the first quasi-steady and the following unsteady sequences; this drives the global vaporization process closer to the infinite diffusivity model. Fig. 9(a) and (b) show, respectively, the variation of the normalized average vaporization rates of the first (K_1/K_{1s}) and the second (K_2/K_{2s}) quasi-steady sequences, where K_{1s} and K_{2s} are, respectively, the average vaporization rates of the first and the second quasi-steady sequences under stagnant conditions. From these figures we can observe that both K_1/K_{1s} and K_2/K_{2s} increase with increasing turbulent kinetic energy for all mixtures. It is also shown on these figures that the trend of this variation is similar to the one found with single mono-component droplets [20] confirming that the effect of turbulence is limited to evacuation and dispersion of the fuel vapor from the vicinity of the droplet surface to its surrounding environment, as the increase of the turbulence level does not involve further increase of the vaporization rate. But this effect itself is very important in preventing the saturation phenomenon which might slow down the vaporization process. However, for a given turbulent kinetic energy, the normalized average vaporization rate for the second quasi-steady sequence remains practically unchanged for different mixture compositions (see Fig. 9(b)). The normalized average vaporization rate for the first quasi-steady sequence increases with decreasing volume fraction of *n*-heptane in the mixture (see Fig. 9(a)). This effect can be explained by the fact that when the volume fraction of the more volatile component (*n*-heptane) in the mixture increases, its vapor concentration at the droplet surface increases too, and thus, the behavior of the mixture approaches that of pure *n*-heptane. However, the decrease of the volume fraction of *n*-heptane, along with the slow mass diffusivity of the liquid phase, lowers the vapor concentration of *n*-heptane on the droplet surface. As a consequence, the least volatile component (*n*-decane) also controls the vaporization process during the first

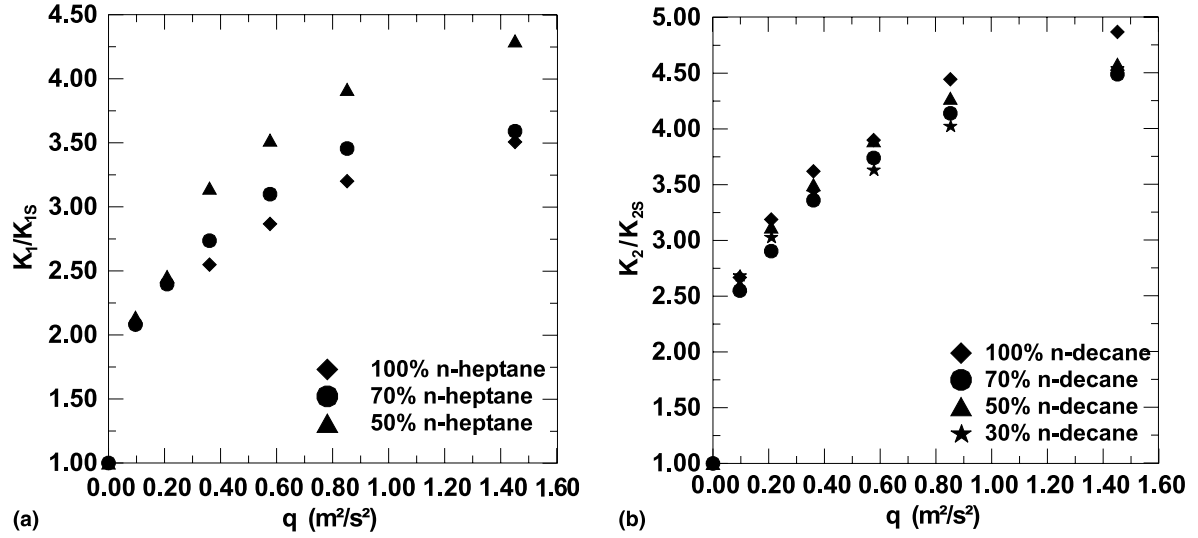

Fig. 9. Variation of the normalized average droplet vaporization rates for the first (9a) and the second (9b) quasi-steady sequences versus turbulent kinetic energy, for three mixtures.

quasi-steady sequence. This explanation is supported by the results obtained with the mono-component droplet, indicating that the turbulence principally influences the least volatile component [20].

Fig. 10 shows the variation of $(K/K_s - 1)$ for two mixtures versus the parameter $Re_t^{2/3}Sc^2$. The average vaporization rates of the first (K_1) and the second (K_2) quasi-steady sequences are displayed together on this figure; they are normalized, respectively, by K_{1s} and K_{2s}. The figure clearly shows that the turbulent vaporization correlation proposed for mono-component droplets also hold for bi-component droplets. The slope of the straight line is again approximately 0.02, as for mono-component droplets. Notice that the Schmidt number for the first steady sequence is estimated using the following equation: $X(Sc)_{\text{heptane}} + (1 - X)(Sc)_{\text{decane}}$. With X being the initial volume fraction of *n*-heptane in the mixture. For the second steady sequence however, only the Schmidt number, Sc, of *n*-decane was considered as the vaporization rate of this sequence is found to be similar to that of *n*-decane. In the present investigation the Schmidt number for *n*-heptane and *n*-decane were calculated at air room temperature to be equal to 2.30 and 2.90, respectively. The present results also differ from those presented in [19], where a much weaker influence of turbulence on bi-component droplet vaporization was reported. In these previous experiments, however, grid turbulence was superimposed on a strong mean convective flow, so that the global vaporization process was controlled by the mean convection effect, rather than by the pure turbulence effect, as is the case in the present study.

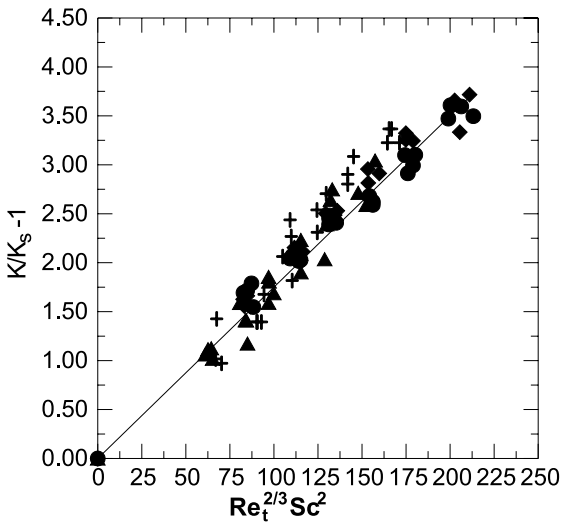

Fig. 10. Variation of the normalized average droplet vaporization rates of the first and second steady sequences for the bi-component droplet of *n*-heptane/*n*-decane mixture versus $Re_t^{2/3}Sc^2$. (+) 50% *n*-heptane $(K_1/K_{1s} - 1)$; (▲) 70% *n*-heptane $(K_1/K_{1s} - 1)$; (●) 30% *n*-decane $(K_2/K_{2s} - 1)$; (◆) 50% *n*-decane $(K_2/K_{2s} - 1)$.

4. Summary and conclusions

Vaporization of single mono- and bi-component *n*-alkane droplets in homogeneous, isotropic and zero-mean velocity turbulence has been investigated under room temperature and pressure conditions. A fan-stirred

turbulence chamber produces the required turbulence characteristics, which are fully characterized by two-component, one and two-point LDV measurements. The vaporization of fiber suspended droplets of five *n*-alkanes and of their bi-component mixtures subjected to varying turbulence energy levels is investigated by imaging techniques. For all experiments, the turbulent energetic (integral) length scales are about 5 times larger than the initial droplet diameter.

For mono-component droplets, the d^2-law holds for all fuels and turbulent kinetic energies explored here. The vaporization rates increase with the turbulent kinetic energy; however, the lowest volatility fuels exhibit a larger increase of the relative vaporization rate K/K_s. Bi-component droplets exhibit a sequential vaporization behavior for all mixtures and turbulent kinetic energies. The instantaneous vaporization rates (or instantaneous liquid phase Peclet numbers) increase with increasing the turbulent kinetic energy and increasing volume fraction of the highest volatility component. As for mono-component droplet vaporization the normalized averaged droplet vaporization rates for bi-component droplets display a trend towards a plateau at higher turbulence kinetic energy levels confirming that turbulence effect is limited to disperse the fuel vapor away from the droplet surface once this vapor is formed.

The experimental results are used to propose a global correlation to account for turbulence effects on the vaporization of mono- and bi-component suspended liquid droplets. This correlation is expressed as $K/K_s = 1 + 0.02Re_t^{2/3}Sc^2$; it is capable of predicting the averaged vaporization rate of liquid droplets evaporating under isotropic and homogeneous turbulence with zero-mean velocity.

Acknowledgements

This work is funded in part by the Commission of the European Communities in the framework of the JOULE II Program (sub-program Energy Conservation and Utilization), by the Swedish National Board for Industrial and Technical Development (NUTEK), by the Austrian Government (FFF) and by EUCAR (Fiat, Peugeot SA, Renault, Rover, Volkswagen and Volvo). Additional support of the Mission Scientifique (DSPT8) of the French Ministry of Higher Education and Research, the Conseil Regional Centre and the CNRS is acknowledged.

References

[1] C.K. Law, Recent advances in droplet vaporization and combustion, Prog. Energy Combust. Sci. 8 (1982) 171–201.
[2] W.A. Sirignano, Fuel droplet vaporization and spray combustion theory, Prog. Energy Combust. Sci. 9 (1983) 291–322.
[3] G.M. Faeth, Evaporation and combustion of sprays, Prog. Energy Combust. Sci. 9 (1983) 1–76.
[4] G.M. Faeth, Mixing transport and combustion in sprays, Prog. Energy Combust. Sci. 13 (1987) 293–345.
[5] D. Stepowski, A. Cessou, P. Goix, Flame stabilization and OH fluorescence mapping of the combustion structures in the near filed of spray jet, Combust. Flame 99 (1994) 516–522.
[6] J.P. Delplanque, W.A. Sirignano, Boundary layer stripping effects on droplet transcritical convective vaporization, Atomization Sprays 4 (1994) 325–349.
[7] N. Frössling, Gerlands Beitr. Geophys. 52 (1938) 170–216.
[8] W.E. Ranz, W.R. Marshall Jr., Evaporation from drops, JR. Chem. Eng. Prog., Part II 48 (1952) 173–180.
[9] W.A. Sirignano, Spray combustion in a turbulent environment, U.S.–Italy Joint Workshop on Heat Transfer and Combustion, Pisa, Italy, September 1982.
[10] I. Gökalp, C. Chauveau, O. Simon, X. Chesneau, Mass transfer from liquid fuel droplets in turbulent flow, Combust. Flame 89 (1992) 286–298.
[11] A.S. Sokolik, V.P. Karpov, E.S. Semenov, Fiz. Goreniya Vzyva 3 (1967) 61–76.
[12] R.G. Abdel-Gayed, D. Bradley, Dependence of turbulent burning velocity on turbulent Reynolds number and ratio of laminar burning velocity to r.m.s. turbulent velocity, in: Sixteenth Symposium (International) on Combustion, The Combustion Institute, Pittsburgh, 1976, pp. 1725–1735.
[13] R.G. Abdel-Gayed, K.J. Al-Khishali, D. Bradley, Turbulent burning velocities and flame straining in explosions, Proc. R. Soc. London A 391 (1984) 393–414.
[14] T.D. Fansler, E.G. Groff, Turbulence characteristics of a fan-stirred combustion vessel, Combust. Flame 80 (1990) 350–354.
[15] S. Kwon, M.-S. Wu, J.F. Driscoll, G.M. Faeth, Flame surface properties of premixed flames in isotropic turbulence: measurements and numerical simulations, Combust. Flame 88 (1992) 221–238.
[16] M. Birouk, Influence de la turbulence homogène et isotrope sur la vaporisation et la combustion des gouttes de combustibles liquids, Ph.D. Thesis, University of Orléans, France, 1996.
[17] A.T. Shih, C.M. Megaridis, Suspended droplet evaporation modeling in a laminar convective environment, Combust. Flame 102 (1995) 256–270.
[18] G.C. Jackson, C.T. Avedisian, J.C. Yang, Observation of soot during droplet combustion at low gravity: heptane and heptane/monochloroalkane mixtures, Int. J. Heat Mass Transfer 35 (1992) 2017–2033.
[19] I. Gökalp, C. Chauveau, H. Berrekam, N.A. Ramos-Arroyo, Vaporization of miscible binary fuel droplets under laminar and turbulent convective conditions, Atomization Sprays 4 (1994) 661–676.
[20] M. Birouk, C. Chauveau, B. Sarh, A. Quilgars, I. Gökalp, Turbulence effects on the vaporization of monocomponent single droplets, Combust. Sci. Technol. 113–114 (1996) 413–428.

[21] D.A. Frank-Kameneskii, Diffusion and Heat Transfer in Chemical Kinetics, second ed., Plenum Press, New York, 1969.

[22] A. Makino, C.K. Law, On the controlling parameter in the gasification behaviour of multicomponent droplets, Combust. Flame 73 (1988) 331–336.